Progress in Natural Science: Materials International 2012;22(6):639–643

Chinese Materials Research Society

Progress in Natural Science: Materials International

www.elsevier.com/locate/pnsmi
www.sciencedirect.com

ORIGINAL RESEARCH

Enhanced photocatalytic activity of sponge-like $ZnFe_2O_4$ synthesized by solution combustion method

Song Sun[a,b], Xiaoyan Yang[b], Yi Zhang[b], Fan Zhang[b], Jianjun Ding[a,b], Jun Bao[a,b,*], Chen Gao[a,b]

[a]*CAS Key Laboratory of Materials for Energy Conversion, Department of Materials Science and Engineering, University of Science and Technology of China, Hefei, Anhui 230026, China*
[b]*National Synchrotron Radiation Laboratory & School of Nuclear Science and Technology, University of Science and Technology of China, Hefei, Anhui 230029, China*

Received 3 August 2012; accepted 7 October 2012
Available online 9 January 2013

KEYWORDS

Zinc ferrite;
Photocatalysis;
Solution combustion;
Infrared thermal image

Abstract A kind of cubic $ZnFe_2O_4$ with spinel structure was synthesized by an improved solution combustion method via a facile and environmentally friendly pathway and their photocatalytic activity under visible light radiation was investigated. The particle synthesized under the ignition temperature of 573 K has a pure phase. While a small amount impurities, α-Fe_2O_3 and ZnO, were formed in the sample during the combustion process at higher ignition temperature of 623 K. The synthesized $ZnFe_2O_4$ has a sponge-like porous structure and wide absorption in the visible-light region. The impurities α-Fe_2O_3 and ZnO formed in the sample probably enhance the reduction and oxidation ability and promote the separation of photo-generated electrons and holes. Comparing with $ZnFe_2O_4$ synthesized by the conventional solid state reaction, the $ZnFe_2O_4$ derived by solution combustion method showed the better photocatalytic activity under visible light radiation.

1. Introduction

Since Fujishima and Honda [1] demonstrated the feasibility of photoelectrochemical splitting water and destruction of toxic organic compounds over a single-crystal TiO_2 photoanode under UV light irradiation, extensive attempts have been made for more efficient use of solar energy to get clean hydrogen and solve the environmental pollution by using many potential photocatalysts [2–4]. TiO_2 is the most commonly used semiconductor in photocatalysis because of its high photocatalytic

*Corresponding author at: National Synchrotron Radiation Laboratory & School of Nuclear Science and Technology, University of Science and Technology of China, Hefei, Anhui 230029, China.
Tel.: +86 551 360 7492; fax: +86 551 514 1078.
E-mail address: baoj@ustc.edu.cn (J. Bao).

Peer review under responsibility of Chinese Materials Research Society.

ELSEVIER Production and hosting by Elsevier

1002-0071 © 2013 Chinese Materials Research Society. Production and hosting by Elsevier Ltd. All rights reserved.
http://dx.doi.org/10.1016/j.pnsc.2012.11.008

activity, chemical stability, low cost and environmental friendliness [4,5]. However, the major drawback of TiO_2 photocatalyst is that its high efficiency occurred only under UV light irradiation due to its wide bandgap energy (3.0–3.2 eV). On the other hand, because most TiO_2 photocatalysts reactions to degrade wastewater were carried out in a relatively interference-free environment in the laboratory, the filtration and collecting of used TiO_2 after photodegradation in wastewater also should be considered. Therefore, as investigators pointed out, more efforts have been made not only to search for the efficient photocatalyst but also to meet with the realistic industrial requirements [6].

Zinc ferrite ($ZnFe_2O_4$) nanoparticles have aroused much interest owing to their potential applications in gas sensor, magnetic behavior, electrical characteristics and photocatalysis [7–11]. Spinel $ZnFe_2O_4$ offers an advantage of displaying the desirable optical absorption for the narrow bandgap of ~1.9 eV and electronic structure for photocatalytic applications [10,11]. Moreover, according to its magnetic property, the used $ZnFe_2O_4$ powders are easy to collect, which make $ZnFe_2O_4$ become one of the most promising photocatalysts in the field of industrial photodegradation of organic pollutants [12]. However, due to the poor separation efficiency of photo-generated electrons and holes, the photocatalytic activity of pure $ZnFe_2O_4$ is worse than that of anatase TiO_2 [13]. Consequently, many strategies, including the surface modification [14,15], metal ion (e.g. Ag) doping [16], nonmetal ion (e.g. S) doping [17], coupling with other semiconductors [18–21], etc. have been adopted to synthesize $ZnFe_2O_4$-based photocatalysts. Besides that, surface modification and fabrication of nanosized $ZnFe_2O_4$ have been intensively investigated in recent years by using coprecipitation, sonochemical emulsification, sol–gel, mechanical milling, hydrothermal synthesis and combustion method in order to promote the charge-transfer process and increase the surface/volume ratio, and finally promote the photocatalytic activity of $ZnFe_2O_4$. Li et al. [14] reported the enhanced photocatalytic activity for degradation of 4-chlorophenol under visible light over the highly ordered $ZnFe_2O_4$ nanotube arrays synthesized by a sol–gel method. Several groups found that the better activities of the various special nanostructured $ZnFe_2O_4$ particles synthesized via the different hydrothermal process were attributed to the quantum confinement effect and high surface area structures, as compared to bulk $ZnFe_2O_4$ samples [22]. However, in most cases, large amounts of organic salts, surfactants or templates are added in the reactions in order to control the microstructures, causing the expensive costs as well as the production of lots of acid–alkali wastewater containing refractory organics. On the other hand, the harsh reaction conditions for the nucleation and growth of nanoparticles homogenously are generally difficult to achieve. Therefore, a facile and environmentally friendly pathway for the preparation of $ZnFe_2O_4$ nanoparticles is expected. Furthermore, although the physical mechanism of photodegradation over $ZnFe_2O_4$ is commonly explained by the semiconductor photocatalytic theory and relatively well understood, the relationships between morphology, structure and activity still need further studies because the properties of photocatalysts are highly sensitive to the composition, microstructure, processing conditions, etc.

In this work, we reported the synthesis of a porous $ZnFe_2O_4$ by an improved solution combustion method, which has the advantages such as simplicity, rapidness and environmentally friendliness. The structure of the synthesized samples was characterized and their photocatalytic activity under visible light radiation was investigated and compared with bulk $ZnFe_2O_4$ synthesized by conventional solid state reaction.

2. Experimental

2.1. Preparation

$ZnFe_2O_4$ sample was synthesized at a relatively low temperature by a solution combustion method using zinc nitrate and ferrite nitrate as oxidizers and glycine as a fuel. The detailed procedure is as follows: 1.49 g $Zn(NO_3)_2 \cdot 6H_2O$, 4.04 g $Fe(NO_3)_3 \cdot 9H_2O$, and 7.81 g $C_2H_5NO_2$ were dissolved in 65 ml deionized water. In the first heating treatment, the mixed solution was kept at 423 K for 30 min to evaporate the excess water. Secondly, it was heated to a set temperature (573 K, 623 K) in 60 min to ignite the solution combustion. During this period, the fluffy $ZnFe_2O_4$ powders were formed and referred to as $ZnFe_2O_4$-SC573K, $ZnFe_2O_4$-SC623K hereafter. The solution combustion reaction is a complex chemical process and can be affected by the type of fuel, fuel/oxidizer ratio, reaction temperature, etc., therefore these factors have been considered and tested beforehand. For comparison, a $ZnFe_2O_4$ sample was synthesized by the conventional solid-state-reaction (SSR) method and referred as to $ZnFe_2O_4$-SSR [23].

2.2. Characterization

X-ray diffraction (XRD) was performed on a MacScience MXPAHF diffractometer with CuKα radiation ($\lambda = 0.15418$ nm). UV–visible diffuse reflectance spectra (DRS) were measured at room temperature with a Shimadzu DUV-3700 UV–visible spectrophotometer using $BaSO_4$ as the reference, and the reflectance was converted into the absorbance by the Kubella–Munk method to estimate the bandgap of the samples. The solution combustion process was observed and recorded by the Forward Looking Infrared thermal imaging system with a THERMACAM P25 camera and the THERMACAM Reporter 2000 software. Transmission electron microscopy (TEM) images were taken on a HitachiH-800 TEM operating at 200 kV. Scanning electron microscopy (SEM) images were characterized using a scanning electron microscope (JEOL JSM-6700F) with an accelerating voltage of 20 kV.

Photocatalytic activity of the prepared $ZnFe_2O_4$ was evaluated by the degradation of Rhodamine B (RhB) in aqueous solution with a concentration of 40 $\mu mol\ L^{-1}$ under visible light irradiation. A detailed account of the experimental setup has been reported elsewhere [24,25].

3. Results and discussion

Compared with conventional solid state reaction, the solution combustion reaction is a complex chemical process and can be affected by the type of fuel, fuel/oxidizer ratio and especially ignition temperature [25–27]. To achieve an optimal reaction condition, the different ignition temperatures were attempted. XRD patterns of the synthesized $ZnFe_2O_4$ samples are shown in Fig. 1. All the samples are characterized by sharp and symmetric peaks, indicating high degree of crystallization and large particle size. The diffraction peaks at 2θ values of 30.3, 35.5, 42.9, 53.2, 56.9 and 62.5 can be assigned to the reflection

of (220), (311), (400), (511) and (440) planes of the cubic $ZnFe_2O_4$ with spinel structure (JCPDS Card no. 79-1150) [28,29]. It can be seen that the $ZnFe_2O_4$ synthesized by SSR method and SC method with a low ignition temperature of 573 K have a pure phase of spinel structure. While a small amount of impurities, α-Fe_2O_3 and ZnO, are detected in $ZnFe_2O_4$ synthesized by the SC method at the ignition temperature of 623 K. The contents of α-Fe_2O_3 and ZnO were estimated as 4.8 at% and 2.2 at% respectively using the semi-quantitative analysis from XPS results (not shown). The infrared thermal images of the solution during the combustion reaction are shown in Fig. 2. The higher ignition temperature results in a more uneven temperature distribution within the solution. For the solution with a temperature of 623 K, the large temperature difference may cause an uneven distribution of components in the reaction container. As a result, some impurities were formed during the combustion process.

The optical properties of the $ZnFe_2O_4$ samples were investigated by UV–visible absorption spectroscopy. As shown in Fig. 3, $ZnFe_2O_4$-SSR mainly absorbs the light with wavelength below 740 nm, while $ZnFe_2O_4$-SC573K exhibits a slight red-shift of spectral response up to approximately 755 nm. The absorption of $ZnFe_2O_4$ in the visible region can be attributed to the photoexcited electron transition from O 2p level into Fe 3d level since the energy band structures of $ZnFe_2O_4$ are generally defined by considering the O 2p orbital as the valence band and the Fe 3d orbital as the conduction band [28]. A sudden enhancement of absorption in the region from 620 to 730 nm is observed in $ZnFe_2O_4$-SC623K sample, which may be caused by a small amount of isolated α-Fe_2O_3 and ZnO present in the samples [29]. This further reflects the impurity detected in XRD results.

The morphological characteristics of $ZnFe_2O_4$ synthesized by the SC method were characterized by SEM and shown in Fig. 4. SEM photographs show that $ZnFe_2O_4$-SC573K is anomalous sponge-like shape with the pore size about 0.1–4 μm. It can be attributed to the sustained release of gas during the combustion process that promotes formation of the porous structure and rough surface, which is a remarkable characteristic of samples synthesized by the SC method [26,30]. The N_2 adsorption–desorption isotherm of the $ZnFe_2O_4$ (not shown) also shows the mesoporous structure with good homogeneity and fairly small pore sizes of synthesized $ZnFe_2O_4$.

The photocatalytic activities of the $ZnFe_2O_4$ samples were investigated and the results were illustrated in Fig. 5. A blank experiment was carried out first and almost no degradation of RhB was observed, indicating that $ZnFe_2O_4$ photocatalysts are active for RhB photocatalytic degradation under visible light irradiation. The degradation rate reached 74.7% over $ZnFe_2O_4$-SSR, while it was enhanced to 90.1% when $ZnFe_2O_4$-SC573K was used. In this study, the solutions before

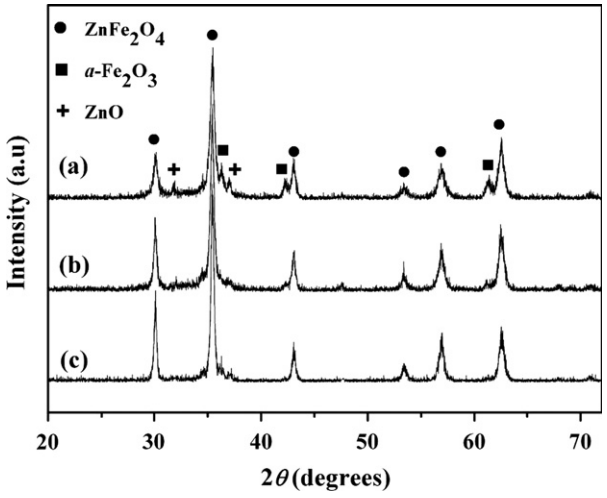

Fig. 1 XRD patterns of (a) $ZnFe_2O_4$ synthesized at the ignition temperature 623 K and (b) 573 K by a solution combustion method, and (c) $ZnFe_2O_4$ synthesized by the conventional solid state reaction.

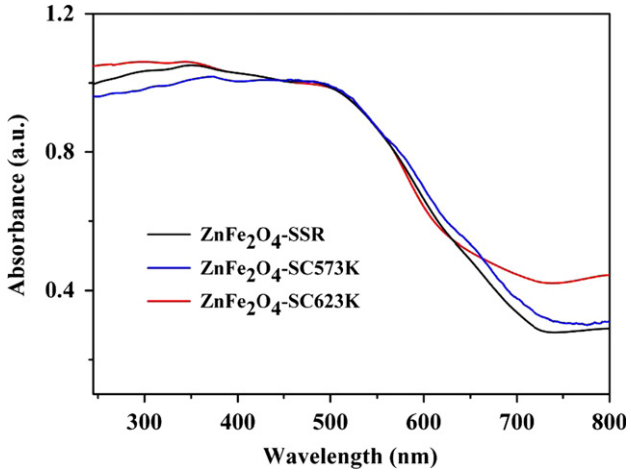

Fig. 3 UV–visible diffuse reflectance spectra of $ZnFe_2O_4$-SSR, $ZnFe_2O_4$-SC573K and $ZnFe_2O_4$-SC623K.

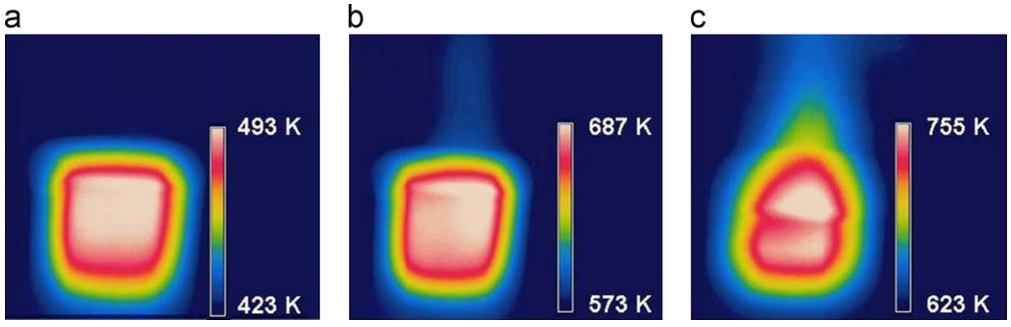

Fig. 2 FLIR images of the solution combustion reaction at (a) the heating stage with the furnace temperature of 423 K, and (b) the ignition stage with the furnace temperature of 573 K and (c) 623 K.

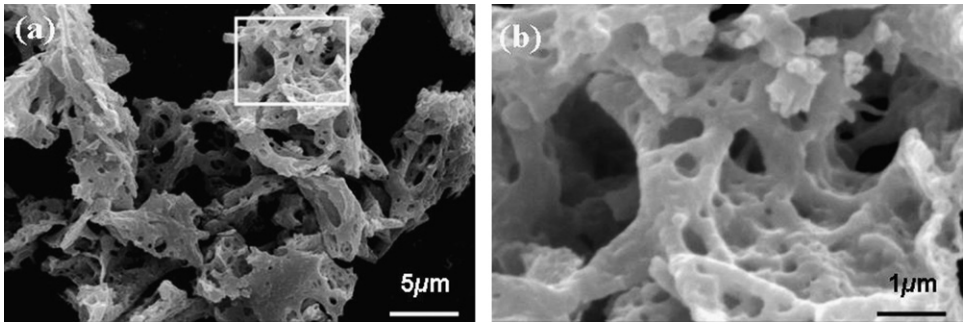

Fig. 4 SEM images of $ZnFe_2O_4$-SC573K, (b) is obtained from the inset square in (a).

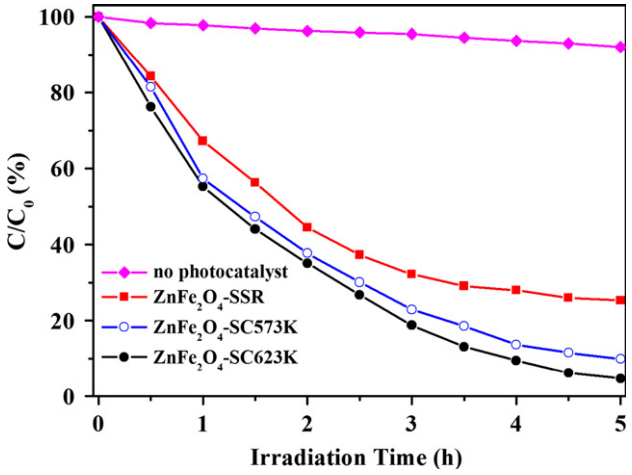

Fig. 5 Photocatalytic degradation of RhB as the normalized concentration change vs. irradiation time using series samples under visible light irradiation.

and after the photocatalytic reaction over $ZnFe_2O_4$ were also analyzed using the ion chromatography in order to determine that the bleaching of RhB is actually due to the photocatalytic mineralization. The concentration of NO_3^- anion, one of the main mineralization products of RhB degradation, was detected to be 70.4 μmol/L (88.0%) and 76.0 μmol/L (95.0%) over $ZnFe_2O_4$-SC573K and $ZnFe_2O_4$-SC623K respectively after the reaction, which is in good agreement with the result in Fig. 5. Generally, the photocatalytic efficiency of a photocatalyst depends on the adsorption ability [31,32], quantum efficiency of the photo-generation of the electron–hole pair, and the diffusion and separation ability of the electron–hole pairs [33], etc. The wide spectral responsibility of $ZnFe_2O_4$ promotes the formation of electron–hole pairs significantly. Besides that, the rough surface and sponge-like morphology may tend to grab the RhB molecules and thus enhance the efficient surface area. Moreover, the special porous structure may decrease the recombination probability of photo-generated electron–hole pairs. The same explanation can be made for the enhanced activity of $ZnFe_2O_4$ synthesized by solution combustion compared with that synthesized by the conventional solid state method. It is noted that $ZnFe_2O_4$-SC623K containing impure phase shows the better activity (95.3%) than $ZnFe_2O_4$-SC573K, which exhibits pure cubic phase with spinel structure. According to the investigations of coupled photocatalysts such as $ZnFe_2O_4$/TiO_2, ZnO/TiO_2 and zinc–iron mixed oxides in literatures [18,34], it is safely deduced that the coupling between $ZnFe_2O_4$, Fe_2O_3 and ZnO is responsible for the enhanced activity of $ZnFe_2O_4$-SC623K. $ZnFe_2O_4$ with narrow band-gap could be easily excited by visible light and induce the generation of electrons from the valence band to the conduction band with simultaneously leaving the holes in the valence band. The photo-generated electrons and holes can recombine or migrate toward the photocatalyst surface where they can react with electron donor or acceptor species adsorbed on the surface of the photocatalyst. Furthermore, due to that the reformed conduction band edge potential of $ZnFe_2O_4$ is more active than that of Fe_2O_3, the photo-generated electrons on the surface of $ZnFe_2O_4$ would easily transfer to the surface of Fe_2O_3. With the consumption of electrons on the surface of Fe_2O_3 in the photocatalytic process, Fe_2O_3 should allow for further transport of photo-generated electrons from $ZnFe_2O_4$. Hence, the photo-generated electrons and holes could be more effectively separated. On the other hand, the energy level at the bottom of the conduction band and the energy level at the top of the valence band determine the reduction ability of electrons and the oxidation ability of holes respectively [4,35]. Therefore, the impurity levels introduced by Fe_2O_3 and ZnO probably enhance the reduction and oxidation ability of $ZnFe_2O_4$-SC623K samples.

4. Conclusions

Through an improved solution combustion method, a kind of pure cubic $ZnFe_2O_4$ with spinel structure was synthesized under the ignition temperature of 573 K. The synthesized $ZnFe_2O_4$ has a sponge-like porous structure and wide absorption in the visible-light region. At higher ignition temperature of 623 K, a small amount of α-Fe_2O_3 and ZnO were formed in the sample during the combustion process, which probably enhance the reduction and oxidation ability and promote the separation of photo-generated electrons. Comparing $ZnFe_2O_4$ synthesized by the conventional solid state reaction, the $ZnFe_2O_4$ synthesized by the solution combustion method showed higher photocatalytic activity for the degradation of RhB under visible light irradiation.

Acknowledgments

This work was supported by National Nature Science Foundation of China (51021091, 20903084 and 11179034), Fundamental Research Funds for the Central Universities (WK2310000020) and China Postdoctoral Science Foundation (2011M501062).

References

[1] A. Fujishima, K. Honda, Electrochemical photolysis of water at a semiconductor electrode, Nature 238 (1972) 37–38.

[2] R. Asahi, T. Morikawa, T. Ohwaki, K. Aoki, Y. Taga, Visible-light photocalysis in nitrogen-doped titanium oxides, Science 293 (2001) 269–271.

[3] S. Sun, J. Bao, C. Gao, J.J. Ding, Photocatalytic degradation of o-xylene in gas phase over M-TiO_2 (M = Ag, Fe, Cu, Co) under different humidity levels, Rare Metals 30 (2011) S147–S152 (Special issue).

[4] M.R. Hoffmann, S.T. Martin, W. Choi, D.W. Bahnemann, Environmental applications of semiconductor photocatalysis, Chemical Reviews 95 (1995) 69–96.

[5] R.M. Alberici, W.F. Jardim, Photocatalytic destruction of VOCs in the gas-phase using titanium dioxide, Applied Catalysis B: Environmental 14 (1997) 55–68.

[6] A. Fujishima, T.N. Rao, D.A. Tryk, Titanium dioxide photocatalysis, Journal of Photochemistry and Photobiology C 1 (2000) 1–21.

[7] F.S. Li, H.B. Wang, L. Wang, J.B. Wang, Magnetic properties of $ZnFe_2O_4$ nanoparticles produced by a low-temperature solid-state reaction method, Journal of Magnetism and Magnetic Materials 309 (2007) 295–299.

[8] N. Ponpandian, A. Narayanasamy, Influence of grain size and structural changes on the electrical properties of nanocrystalline zinc ferrite, Journal of Applied Physics 92 (2002) 2770–2778.

[9] M.P. Pileni, Magnetic fluids: fabrication, magnetic properties, and organization of nanocrystals, Advanced Functional Materials 11 (2001) 323–336.

[10] X.Y. Li, Y. Hou, Q.D. Zhao, L.Z. Wang, A general, one-step and template-free synthesis of sphere-like zinc ferrite nanostructures with enhanced photocatalytic activity for dye degradation, Journal of Colloid and Interface Science 358 (2011) 102–108.

[11] S.W. Cao, Y.J. Zhu, G.F. Cheng, Y.H. Huang, $ZnFe_2O_4$ nanoparticles: microwave–hydrothermal ionic liquid synthesis and photocatalytic property over phenol, Journal of Hazardous Materials 171 (2009) 431–435.

[12] Y.S. Fu, X. Wang, Magnetically separable $ZnFe_2O_4$–graphene catalyst and its high photocatalytic performance under visible light irradiation, Industrial and Engineering Chemistry Research 50 (2011) 7210–7218.

[13] P. Cheng, W. Li, T.L. Zhou, Y.P. Jin, M.Y. Gu, Physical and photocatalytic properties of zinc ferrite doped titania under visible light irradiation, Journal of Photochemistry and Photobiology C 168 (2004) 97–101.

[14] X.Y. Li, Y. Hou, Q.D. Zhao, W. Teng, X.J. Hu, G.H. Chen, Capability of novel $ZnFe_2O_4$ nanotube arrays for simulated-sunlight induced degradation of 4-chlorophenol, Chemosphere 82 (2011) 581–586.

[15] C.H. Chen, Y.H. Liang, W.D. Zhang, $ZnFe_2O_4$/MWCNTs composite with enhanced photocatalytic activity under visible-light irradiation, Journal of Alloys and Compounds 501 (2010) 168–172.

[16] X.B. Cao, L. Gu, X.M. Lan, C. Zhao, D. Yao, W.J. Sheng, Spinel $ZnFe_2O_4$ nanoplates embedded with Ag clusters: preparation, characterization, and photocatalytic application, Materials Chemistry and Physics 106 (2007) 175–180.

[17] L.J. Liu, G.L. Zhang, L. Wang, T. Huang, L. Qin, Highly active S-modified $ZnFe_2O_4$ heterogeneous catalyst and its photo-fenton behavior under UV–visible irradiation, Industrial and Engineering Chemistry Research 50 (2011) 7219–7227.

[18] X.Y. Li, Y. Hou, Q.D. Zhao, G.H. Chen, Synthesis and photo-induced charge transfer properties of $ZnFe_2O_4$–sensitized TiO_2 nanotube-array electrode, Langmuir 27 (2011) 3113–3120.

[19] L. Kong, Z. Jiang, T. Xiao, L. Lu, M.O. Jones, P.P. Edwards, Exceptional visible-light-driven photocatalytic activity over BiOBr–$ZnFe_2O_4$ heterojunctions, Chemical Communications 47 (2011) 5512–5514.

[20] G.G. Liu, X.Z. Zhang, Y.J. Xu, X.S. Niu, L.Q. Zheng, X.J. Ding, Effect of $ZnFe_2O_4$ doping on the photocatalytic activity of TiO_2, Chemosphere 55 (2004) 1287–1291.

[21] Z.H. Yuan, L.D. Zhang, Synthesis, characterization and photocatalytic activity of $ZnFe_2O_4$/TiO_2 nanocomposite, Journal of Materials Chemistry 11 (2001) 1265–1268.

[22] G.L. Fan, Z.J. Gu, L. Yang, F. Li, Nanocrystalline zinc ferrite photocatalysts formed using the colloid mill and hydrothermal technique, Chemical Engineering Journal 155 (2009) 534–541.

[23] S. Zahi, A.R. Daud, M. Hashim, A comparative study of nickel–zinc ferrites by sol–gel route and solid-state reaction, Materials Chemistry and Physics 106 (2007) 452–456.

[24] S. Sun, J.J. Ding, J. Bao, C. Gao, Z.M. Qi, X.Y. Yang, B. He, C.X. Li, Photocatalytic degradation of gaseous toluene on Fe–TiO_2 under visible light irradiation: a study on the structure, activity and deactivation mechanism, Applied Surface Science 258 (2012) 5031–5037.

[25] J.J. Ding, S. Sun, J. Bao, Z.L. Luo, C. Gao, Synthesis of $CaIn_2O_4$ rods and its photocatalytic performance under visible-light irradiation, Catalysis Letters 130 (2009) 147–153.

[26] J.J. Moore, H.J. Feng, Combustion synthesis of advanced materials: part 2–reaction parameters, Progress in Materials Science 39 (243–273) (1995) 275–316.

[27] K.C. Patil, Advanced ceramics: combustion synthesis and properties, Bulletin of Material Science 16 (1993) 533–541.

[28] H. Lv, L. Ma, P. Zeng, D. Ke, T. Peng, Synthesis of floriated $ZnFe_2O_4$ with porous nanorod structures and its photocatalytic hydrogen production under visible light, Journal of Materials Chemistry 20 (2010) 3665–3672.

[29] M.A. Valenzuela, P. Bosch, J. Jimenez-Becerrill, O. Quiroz, A.I. Paez, Preparation, characterization and photocatalytic activity of ZnO, Fe_2O_3 and $ZnFe_2O_4$, Journal of Photochemistry and Photobiology C 148 (2002) 177–182.

[30] H. Xue, Z.H. Li, X.X. Wang, X.Z. Fu, Facile synthesis of nanocrystalline zinc ferrite via a self-propagating combustion method, Materials Letters 61 (2007) 347–350.

[31] F.B. Li, X.Z. Li, C.H. Ao, S.C. Lee, M.F. Hou, Enhanced photocatalytic degradation of VOCs using Ln^{3+}–TiO_2 catalysts for indoor air purification, Chemosphere 59 (2005) 787–800.

[32] K.T. Ranjit, I. Willner, S.H. Bossmann, A.M. Braun, Lanthanide oxide doped titanium dioxide photocatalysts: effective photocatalysts for the enhanced degradation of salicylic acid and t-cinnamic acid, Journal of Catalysis 204 (2001) 305–313.

[33] J.J. Kelly, E.S. Kooij, E.A. Meulenkamp, Luminescence studies of semiconductor electrodes, Electrochimica Acta 45 (1999) 561–574.

[34] G.K. Pradhan, S. Martha, K.M. Parida, Synthesis of multifunctional nanostructured zinc–iron mixed oxide photocatalyst by a simple solution-combustion technique, ACS Applied Materials and Interfaces 4 (2012) 707–713.

[35] M.I. Litter, Heterogeneous photocatalysis transition metal ions in photocatalytic systems, Applied Catalysis B: Environmental 23 (1999) 89–114.